

Cite this: *Energy Environ. Sci.*,  
2024, 17, 2492

# Light-induced quinone conformation of polymer donors toward 19.9% efficiency organic solar cells†

Chuanhang Guo,<sup>a</sup> Yuandong Sun,<sup>a</sup> Liang Wang,<sup>a</sup> Chenhao Liu,<sup>a</sup> Chen Chen,<sup>a</sup>  
Jingchao Cheng,<sup>b</sup> Weiyi Xia,<sup>a</sup> Zirui Gan,<sup>a</sup> Jing Zhou,<sup>a</sup> Zhenghong Chen,<sup>a</sup>  
Jinpeng Zhou,<sup>a</sup> Dan Liu,<sup>a</sup> Jingxing Guo,<sup>c</sup> Wei Li<sup>a</sup> and Tao Wang \*<sup>ab</sup>

Modulating the self-assembly process of polymer donors is crucial to acquire an ideal morphology of the photoactive layer for efficient photovoltaics, however, this always requires complicated chemical synthesis or comprehensive physical treatments. In this work, a facile morphology optimization method was realized by irradiating polymer solutions with a 365 nm UV-light for achieving enhanced intermolecular ordering of polymer donors. Fourier transform infrared spectroscopy and Raman spectroscopy reveal that light irradiation can disrupt the aromatic conformation of polymers and induce the formation of a rigid quinone structure. Synchrotron X-ray diffraction suggests that the rigid quinone skeleton improves the planarity of polymers to form compact aggregates with enhanced  $\pi$ - $\pi$  stacking in their pristine and blend thin films with non-fullerene acceptor L8-BO. As a result, both PM6:L8-BO and D18:L8-BO based devices exhibited enhanced carrier transport and suppressed recombination, leading to power conversion efficiency (PCE) enhancements from 18.8% to 19.7% and from 18.9% to 19.6%. The versatility of this strategy is also verified using more polymer donors including PTB7-Th and PBDB-T. Impressively, the D18:PM6:L8-BO ternary system delivered a maximum PCE of 19.9%, which is among the highest value of single-junction organic solar cells.

Received 6th February 2024,  
Accepted 4th March 2024

DOI: 10.1039/d4ee00605d

rsc.li/ees

## Broader context

Organic solar cells (OSCs) are considered as a promising next-generation photovoltaic technology, and with the continuous development of materials design and device engineering, OSCs can exhibit their maximum performance. However, OSCs are still suffering from low carrier mobility and strong carrier recombination due to their low structural order. Hence, various chemical and physical strategies have been used to enhance the structural order of organic semiconductors to establish efficient charge transport tunnels. With the expectations of industrialization, developing a facile and versatile method is vital for achieving viable organic photovoltaics. In this work, we report a facile aggregation control of conjugated polymer donors PM6, D18, PBDB-T and PTB7-Th *via* a simple light-induced conformation conversion strategy to construct a rigid polymer skeleton, which leads to a transition of their aromatic configuration into a rigid quinone configuration in the solution state and the quinone conformation facilitated enhanced molecular  $\pi$ - $\pi$  stacking and more compact aggregation in solid films. This helps to achieve enhanced charge transport to improve device PCE in four different OSC systems to demonstrate its universality. As a result, improved device efficiency is achieved with simultaneously enhanced fill factor (FF) and short-circuit current density ( $J_{sc}$ ) and a maximum PCE of 19.9% can be achieved in the D18:PM6:L8-BO ternary device. This work provides a rational guide for optimizing OSC performance *via* transforming the molecular structure with a physical method and expands its universality.

## 1 Introduction

As the next generation of photovoltaic technology, organic photovoltaics have drawn significant attention in recent decades due to their advantages of lightweight,<sup>1</sup> flexibility<sup>2</sup> and tunable optoelectronic properties.<sup>3</sup> With the continuous development of materials design and device engineering, a power conversion efficiency (PCE) of 19% has been achieved in single-junction organic solar cells (OSCs).<sup>4–10</sup> However, different from inorganic

<sup>a</sup> School of Materials Science and Engineering, Wuhan University of Technology, Wuhan 430070, China. E-mail: twang@whut.edu.cn

<sup>b</sup> School of Materials and Microelectronics, Wuhan University of Technology, Wuhan 430070, China

<sup>c</sup> School of Chemistry, Chemical Engineering and Life Sciences, Wuhan University of Technology, Wuhan 430070, China

† Electronic supplementary information (ESI) available. See DOI: <https://doi.org/10.1039/d4ee00605d>

crystalline materials, organic semiconductors are often organized through weak non-covalent bonds and exhibit low structural order.<sup>11,12</sup> As such, charge transport in organic semiconductors is *via* the hopping of carriers along their conjugated  $\pi$ - $\pi$  electron clouds and always inefficient compared with that in their inorganic counterparts.<sup>13,14</sup>

Enhancing the structural order of organic semiconductors to establish efficient charge transport tunnels plays a vital role in further enhancing their photovoltaic performance.<sup>15-17</sup> To realize that, strategies including chemical structure modifications, regioregularity and molecular weight design of polymers,<sup>18,19</sup> film deposition control such as hot-solution or hot-substrate casting,<sup>20,21</sup> and post treatments including thermal annealing (TA) and solvent vapor annealing (SVA) have been widely used in the field.<sup>22,23</sup> Nevertheless, these complicated chemical and physical treatments do not meet the expectations of industrialization.<sup>24</sup>

During the fabrication of photoactive layers of OSCs, the organic semiconducting molecules first undergo a swelling and dissolving process which is driven by their interactions with solvent molecules.<sup>25-27</sup> Modulating the self-assembly behavior

of photovoltaic materials during film formation *via* controlling the solution state has been considered as a facile and easy-to-process method, and has attracted extensive interest very recently.<sup>28-30</sup> For example, the replacement of a “poor solvent” with a “good solvent” can lead polymers to exhibit strong intrinsic preaggregation and further improve their domain size and purity after film-formation, thus facilitating efficient charge transport in their photovoltaic films.<sup>31</sup> Temperature-dependent aggregation properties can also give polymers different aggregation behavior in the solution-state and allow them to organize into distinct molecular order in solid films.<sup>32</sup> However, although significant advances have been achieved using the above methods, the solvent system selection and temperature control also complicate the pre-aggregation and final morphology optimization of the photoactive layer. Hence, developing a facile and versatile method is vital for achieving viable organic photovoltaics.

In this work, we propose a light-induced conformation conversion strategy to construct a rigid polymer skeleton by transforming its aromatic configuration into rigid quinone configuration, as confirmed by Fourier transform infrared (FT-IR)

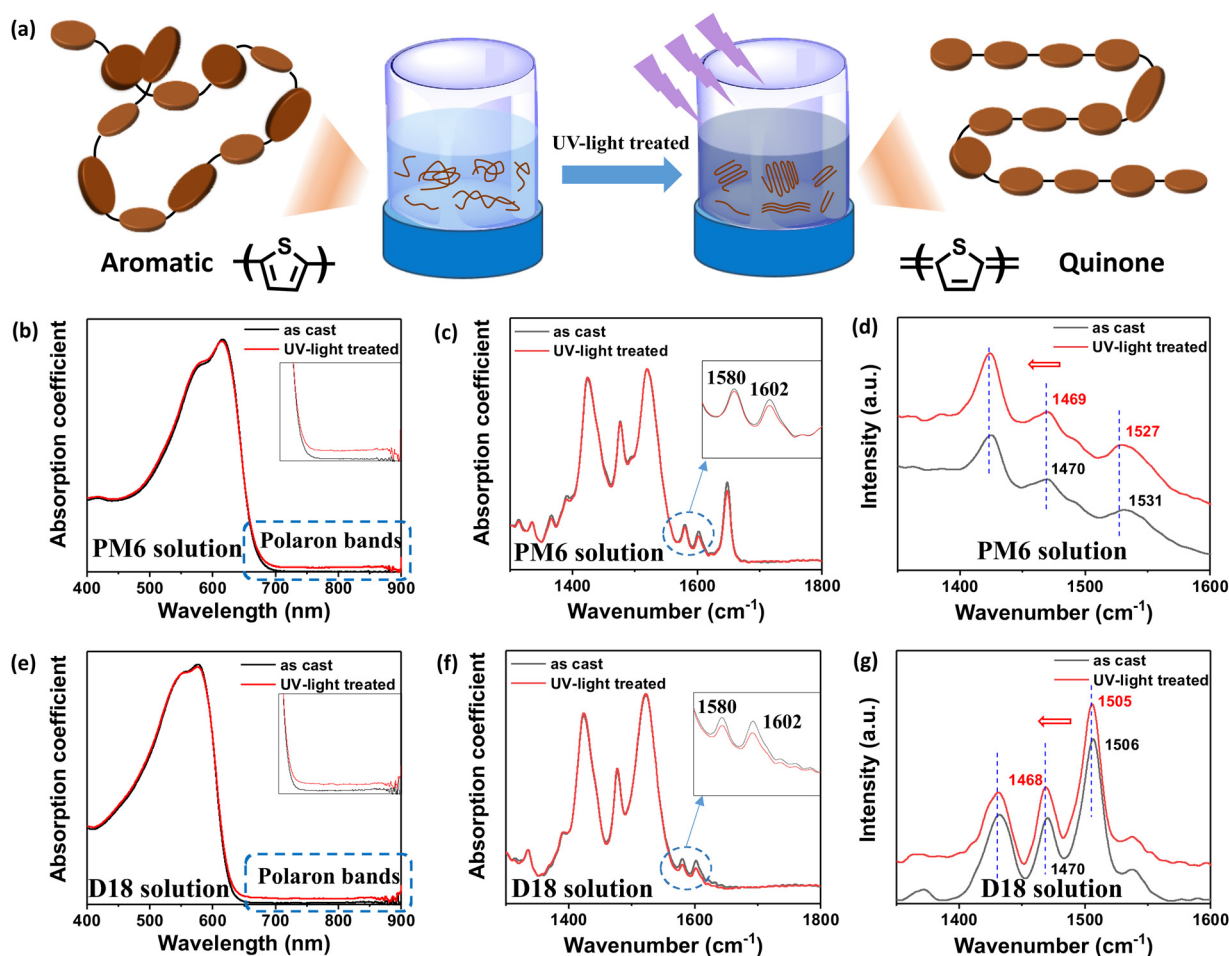


Fig. 1 (a) Schematic diagram of light-induced pre-aggregation of a polymer, where the solution vial was placed invertedly with a UV light cast through the top. (b) Absorption spectra, (c) Fourier transform infrared (FT-IR) spectra and (d) Raman spectra of the PM6 solution obtained with different treatments. (e) Absorption spectra, (f) FT-IR spectra and (g) Raman spectra of D18 solution obtained with different treatments.

spectroscopy and Raman spectroscopy. Through comprehensive X-ray diffraction and morphology characterization, we found that the quinone conformation facilitated enhanced molecular  $\pi$ - $\pi$  stacking and more compact aggregation in solid films, leading to enhanced charge transport. As a result, improved device efficiency is observed in both PM6:L8-BO and D18:L8-BO OSCs, with a simultaneously enhanced fill factor (FF) and short-circuit current density ( $J_{sc}$ ). The versatility of this method is further validated in a range of photovoltaic systems, with a maximum PCE of 19.9% achieved in the D18:PM6:L8-BO ternary device. Our method offers a facile physical treatment of the photovoltaic solution that is converted to a favorable morphology in the solid photoactive layer for achieving the milestone power conversion efficiency of 20%.

Moreover, without any comprehensive chemical synthesis and physical manipulations, we envisage that it can be integrated with the roll-to-roll or slot-die manufacturing process, presenting its potential for practical application in large-scale production.

## 2 Results and discussion

As shown in Fig. 1a, to modulate the structural conformation of polymer donors, a 365 nm UV light source with a power of  $5 \text{ mW cm}^{-2}$  was utilized to irradiate the PM6<sup>33</sup> or D18<sup>34</sup> (see the chemical structure in Fig. S1, ESI<sup>†</sup>) solution stored in a glass vial (transmittance over 90% at 365 nm). Upon the UV-light

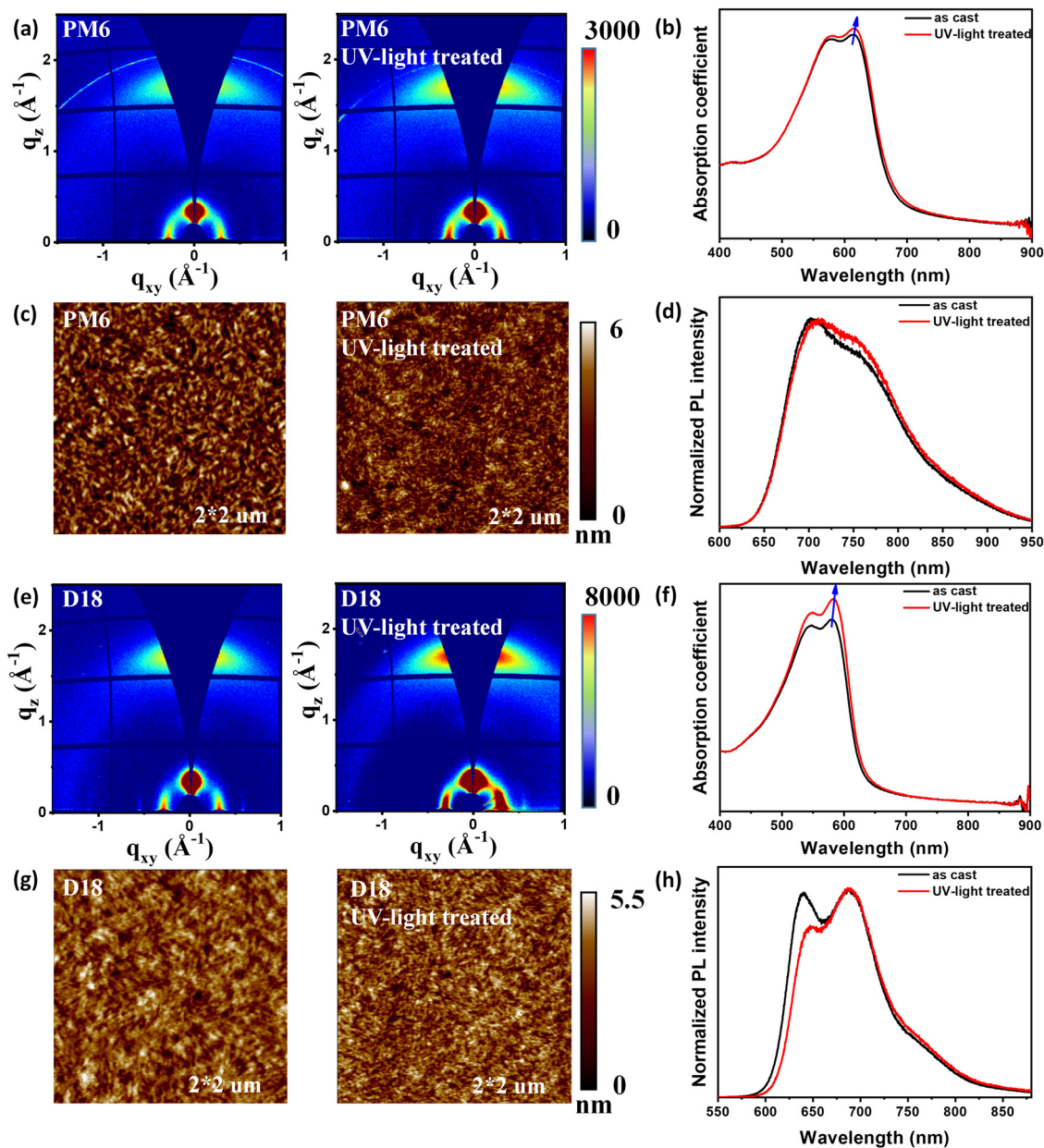


Fig. 2 2D Grazing-incidence wide-angle X-ray scattering (GIWAXS) patterns of (a) PM6 and (e) D18 films. Atomic force microscopy (AFM) height images of (c) PM6 and (g) D18 films. UV-vis spectra of (b) PM6 and (f) D18 films. PL spectra of (d) PM6 and (h) D18 films with or without UV-light treatment.

treatment, the absorption spectra of PM6 and D18 CF solutions exhibited notable changes across the near-infrared region (Fig. 1b and e). These observed absorption bands can be attributed to the formation of carrier-polaron-excitations,<sup>35,36</sup> which are normally aroused by the transitions of delocalized polarons in ordered polymer phases upon external chemical doping or donor-acceptor photophysical interactions.<sup>37-39</sup> Here, we envisage that the polymer donors can transform from an aromatic conformation in the ground state to a quinone conformation in the excited state.

To confirm this conformation conversion, FT-IR and Raman spectra were obtained for the PM6 and D18 solutions with or without UV-light treatment. As shown in Fig. 1c and f, both PM6 and D18 solutions exhibit FT-IR signals at 1580 and 1602  $\text{cm}^{-1}$ , corresponding to the stretching vibrations of C=C in the aromatic ring. After UV-light treatment, decreased intensities are observed for these two peaks, suggesting the disruption of the aromatic conformation.<sup>40</sup> Meanwhile, from their Raman spectra, blue-shifts were observed for the characteristic peaks of the benzo[1,2-*b*:4,5-*b'*]dithiophene-

thiophene (BDT-T) linkage of PM6 and D18 (Fig. 1d and g), suggesting a decreased dihedral angle of the BDT-T plane which is indicative of the transformation from the aromatic to a quinone structure in the PM6 and D18 solutions.<sup>41</sup>

Then the UV-light treated PM6 and D18 solutions were spin-coated into thin films to probe the impact of the quinone conformation on the structural order in the solid state. As shown in Fig. 2, we found that both PM6 and D18 films processed with UV-light show increased grazing-incidence wide-angle X-ray scattering (GIWAXS) intensities of the (100) diffraction spots at  $q_z = 0.30 \text{ \AA}^{-1}$  or  $q_z = 0.31 \text{ \AA}^{-1}$  and the (010)  $\pi$ - $\pi$  stacking crescents at  $q_z = 1.71 \text{ \AA}^{-1}$  or  $q_z = 1.70 \text{ \AA}^{-1}$ , respectively. Meanwhile, the increased  $I_{011}/I_{010}$  ratio in their absorption spectra and their steady-state photoluminance (PL) spectra was also observed when compared with their control films, confirming increased structural order induced by the quinone conformation in the solution state.<sup>42,43</sup> Additionally, this enhanced structural order is supported by their atomic force microscope (AFM) images, where both PM6 and D18 films show denser aggregates on their surface (Fig. 2c and g).

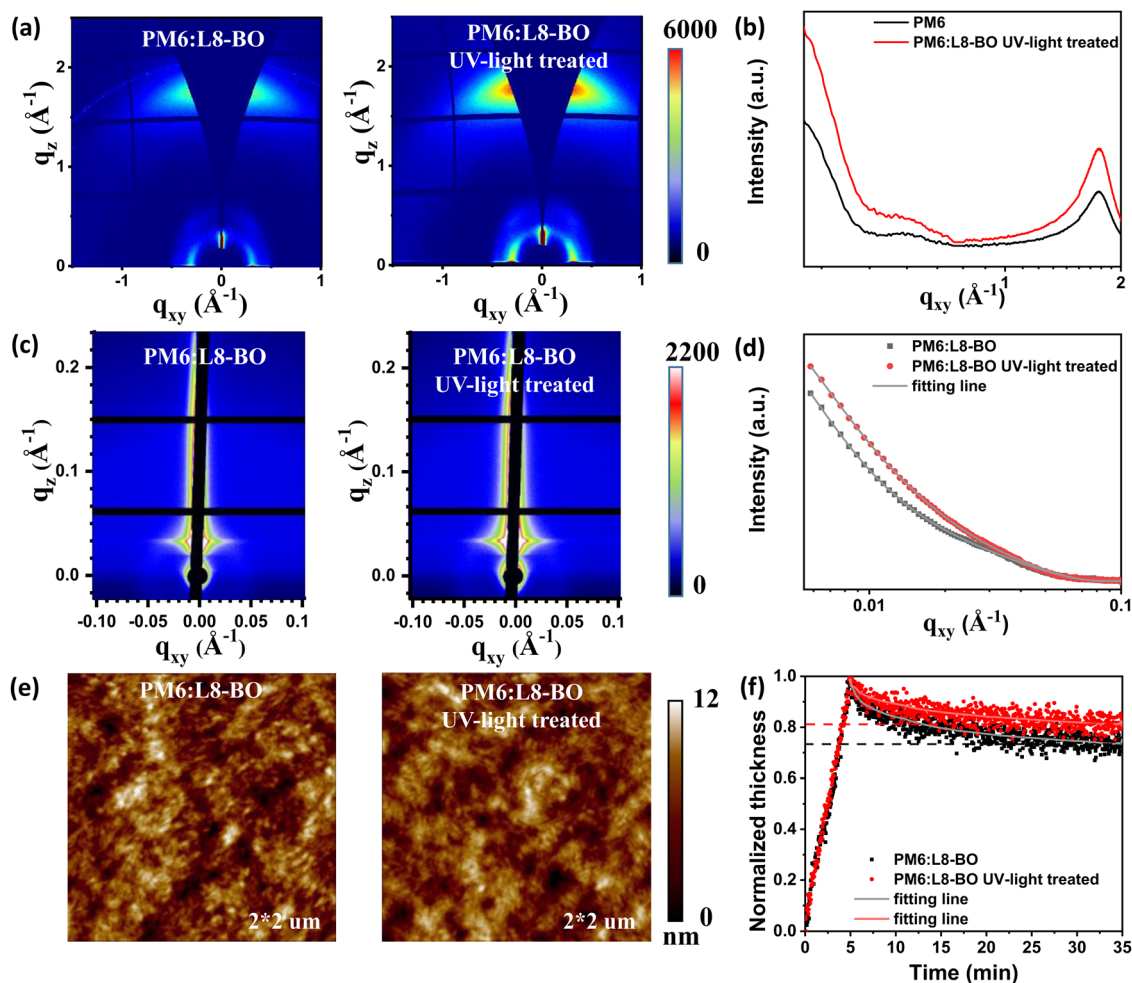


Fig. 3 (a) 2D GIWAXS patterns, (b) 1D GIWAXS profiles along out-of-plane, (c) 2D GISAXS patterns, (d) 1D GISAXS profiles along in-plane, (e) AFM height image and (f) thermal expansion during heating and structural relaxation during isothermal annealing of PM6:L8-BO films with or without UV-light treatment.

**Table 1** GISAXS fitting parameters obtained via a DAB + Fractal model, where the correlation length  $\xi$  refers to the domain size of the donor-rich phase,  $\eta$  and  $D$  represent the correlation length and fractal dimension of acceptors, and  $2R_g$  is regarded as the domain size of the acceptor domain

	$\xi$ (nm)	$\eta$ (nm)	$D$	$2R_g$ (nm)
PM6:L8-BO	26.3	8.5	1.77	26.6
PM6:L8-BO UV light treated	20.9	5.4	2.75	24.5

The PM6 film was further selected to perform grazing-incidence small-angle X-ray scattering (GISAXS) (Fig. S2a–c and Table S1, ESI<sup>†</sup>), and the 1D profile fitting indicates a larger fractal dimensionality ( $D$ ) within the film processed with UV-light, which corresponds to more compact aggregates (experimental and simulation details can be found in the ESI<sup>†</sup>).

To explore the versatility, we extended this UV-light treatment method to PBDB-T and PTB7-Th polymer donors (see the chemical structure in Fig. S1, ESI<sup>†</sup>). As expected, all these films achieved stronger structural order in their solid state according to absorption, PL and AFM measurements (Fig. S3, ESI<sup>†</sup>). Additionally, significantly stronger (100) and (010) diffraction peaks with enlarged crystalline coherence length (CCL) are observed in their GIWAXS patterns (Fig. S4 and S5, detailed GIWAXS data summarized in Table S2, ESI<sup>†</sup>), suggesting their quinone-conformation in the solution state has enhanced the structural order of those polymers in solid thin films.

Then a cutting-edge non-fullerene acceptor L8-BO was selected to match with the above method treated PM6 donor to prepare a heterojunction photoactive layer. As shown in their GIWAXS 2D patterns and 1D profiles in Fig. 3a and b, the reference PM6:L8-BO film shows a (100) diffraction peak at  $q_z = 0.30 \text{ \AA}^{-1}$  and a (010)  $\pi$ - $\pi$  stacking crescent at  $q_z = 1.73 \text{ \AA}^{-1}$ , consistent with previous work.<sup>28</sup> Upon UV-light treatment, pronounced enhancements are observed for both the (100) and (010) peaks, suggesting that the impact of the quinone-conformation in enhancing the structural order of PM6 is still effective with the presence of L8-BO. The D18:L8-BO film presents a similar GIWAXS pattern evolution upon UV light treatment, confirming the versatility of the blend film (Fig. S6, ESI<sup>†</sup>). The nanoscale morphology of the above films was further studied by GISAXS (Fig. 3c and d and Table 1). Compared with the relatively loose aggregation of the reference PM6:L8-BO film with a PM6 domain size ( $\xi$ ) of 26.3 nm and a L8-BO domain size ( $2R_g$ ) of 26.6 nm, the blend film prepared by UV-light treatment presents a higher  $D$  value from 1.77 to 2.75 and slightly smaller

$\xi$  of 20.9 nm and  $2R_g$  of 24.5 nm, suggesting the establishment of a denser aggregation structure, consistent with the AFM height images shown in Fig. 3e.

This more compact aggregation of the photoactive film was also validated by measuring its free volume during structural relaxation at an elevated temperature, in which the film thickness changes were monitored *in situ* using ellipsometry at 150 °C (heated from room temperature at a rate of 25 °C per minute).<sup>44</sup> As shown in Fig. 3f, the blend film prepared with UV-light treated PM6 presents a smaller reduction (which is associated with the molecular rearrangement of the photovoltaic materials toward equilibrium assisted by thermal stress) in thickness during structural relaxation compared to the reference film, suggesting a smaller free volume and denser film was formed during solution casting, consistent with our above analysis.

Then the above films were applied to assemble single-junction OSCs (ITO/2PACz/active layer/PDINN/Ag). As shown in Table 2, the reference PM6:L8-BO and D18:L8-BO based OSCs show maximum PCEs of 18.8% and 18.9%, respectively. While for devices prepared by the UV-light treated PM6 (the optimization process of the UV-light irradiation time is summarized in Table S2, ESI<sup>†</sup>), maximum PCEs of 19.7% and 19.6% were achieved with the increments of the FF from 79.0% to 80.1% and 78.3% to 79.8%,  $J_{SC}$  from 27.0 to 27.5 and 26.6 to 27.2  $\text{mA cm}^{-2}$  in PM6:L8-BO and D18:L8-BO OSCs, respectively (Fig. 4a–c). The external quantum efficiency (EQE) spectra in relation to these best-performing devices are shown in Fig. 4d–f, from which enhanced photon-to-electricity responses from 500 to 700 nm can be observed in all devices prepared by UV-light treated PM6, validating the contribution of the quinone-conformation. The integrated  $J_{SC}$  values obtained from the EQE spectra are summarized in Table 1, only *ca.* 3% less than the  $J_{SC}$  values obtained from  $J$ - $V$  scans, thereby validating the  $J$ - $V$  measurements. More importantly, we further conducted this strategy in the D18:PM6:L8-BO ternary system, and a promising PCE of 19.9% was achieved when UV-light treated D18:PM6 was employed. Additionally, the versatility of this method was further validated using PTB7-Th:L8-BO and PBDB-T:L8-BO systems, in which enhanced photovoltaic performance is achieved as shown in Fig. S7 and Table S4 (ESI<sup>†</sup>).

To probe the charge transport and collection in the above devices, space-charge-limited current (SCLC) method and transient photocurrent (TPC) and transient photovoltage (TPV) measurements were further performed. As shown in Fig. S8 (ESI<sup>†</sup>), devices prepared by UV-light treatment achieve a shorter

**Table 2** Photovoltaic metrics of OSCs with different photoactive layers

OSCs	Condition	PCE <sub>max</sub> (PCE)	FF (%)	$J_{SC}$ ( $\text{mA cm}^{-2}$ )	$J_{cal}$ ( $\text{mA cm}^{-2}$ )	$V_{OC}$ (V)
PM6:L8-BO	as cast	18.8 (18.5 ± 0.3)	79.0	−27.0	26.3	0.89
PM6:L8-BO	UV-light treated	19.7 (19.4 ± 0.2)	80.1	−27.5	26.8	0.89
D18:L8-BO	as cast	18.9 (18.7 ± 0.2)	78.3	−26.6	25.9	0.91
D18:L8-BO	UV-light treated	19.6 (19.4 ± 0.2)	79.8	−27.2	26.4	0.91
D18:20%PM6:L8-BO	as cast	19.3 (19.0 ± 0.2)	79.3	−26.9	26.2	0.90
D18:20%PM6:L8-BO	UV-light treated	19.9 (19.6 ± 0.2)	80.4	−27.5	26.7	0.90

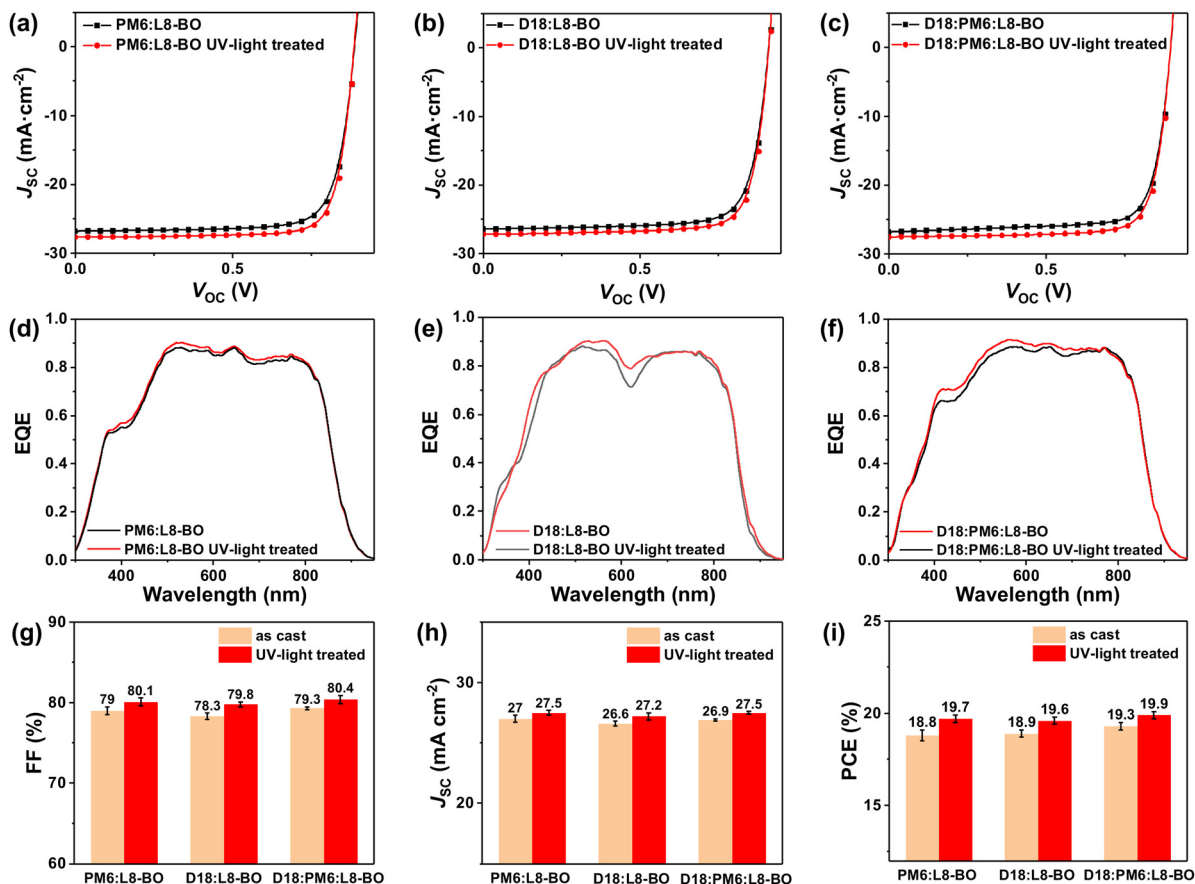


Fig. 4  $J$ - $V$  characteristics of (a) PM6:L8-BO, (b) D18:L8-BO, and (c) D18:PM6:L8-BO based OSCs. EQE spectra of (d) PM6:L8-BO, (e) D18:L8-BO, and (f) D18:PM6:L8-BO based OSCs. The corresponding (g) FF, (h)  $J_{sc}$  and (i) PCE values.

charge extraction time (0.19  $\mu$ s) and a longer carrier lifetime (124  $\mu$ s) compared to 0.22  $\mu$ s and 80  $\mu$ s, respectively, of the PM6:L8-BO reference device, confirming the improved charge extraction and transport processes, which correspond to the enlarged  $J_{sc}$  and FF as shown above. Meanwhile, enhanced hole mobilities are also achieved in all polymer films processed with UV-light treatment (Fig. S9, and summary in Table S5, ESI<sup>†</sup>), confirming the elevated charge transport ability.

### 3 Conclusion

In summary, we reported a facile method of enhancing the structural order of semiconducting polymers through a structural transition from their aromatic to quinone conformation *via* UV-light irradiation. Comprehensive optical and morphological characterization proves that this conformation transition can help to modulate the aggregation behavior of polymers in the subsequent solution casting into solid thin films, leading to enhanced structural order and more compact aggregation for a range of polymers including PM6, D18, PTB7-Th and PDBD-T. As a result, improved photovoltaic performance with enhanced charge transport and suppressed recombination is observed in all these polymer:non-fullerene OSCs, leading to a maximum PCE of 19.9% in the D18:PM6:L8-BO ternary OSC.

### Author contributions

C. G. performed device fabrication and collected data. C. G. and C. C. conducted molecular dynamics simulations. Y. S., W. X. and L. W. performed synchrotron X-ray measurements. C. L., J. C., Z. G., J. Z., Z. C. and J. P. Z. conducted morphology characterization. W. L. and D. L. assisted experimental design and data analysis. All authors were involved in result discussion. C. G., W. L. and T. W. wrote the manuscript, with all authors commenting and revising this paper. T. W. supervised the project.

### Conflicts of interest

The authors declare no conflicts of interest.

### Acknowledgements

This work was supported by the Key Research and Development Program of Hubei Province (2023BAB116) and the National Natural Science Foundation of China (52073221, 52273196, 52203238). We thank beamline BL16B1 at Shanghai Synchrotron Radiation Facility (China) for providing beam times to perform GIWAXS and GISAXS measurements.

## References

- M. Kaltenbrunner, M. S. White, E. D. Glowacki, T. Sekitani, T. Someya, N. S. Sariciftci and S. Bauer, *Nat. Commun.*, 2012, **3**, 770.
- D. Koo, S. Jung, J. Seo, G. Jeong, Y. Choi, J. Lee, S. M. Lee, Y. Cho, M. Jeong, J. Lee, J. Oh, C. Yang and H. Park, *Joule*, 2020, **4**, 1021–1034.
- R. Xia, C. J. Brabec, H. L. Yip and Y. Cao, *Joule*, 2019, **3**, 2241–2254.
- H. Lu, W. Liu, G. Ran, Z. Liang, H. Li, N. Wei, H. Wu, Z. Ma, Y. Liu, W. Zhang, X. Xu and Z. Bo, *Angew. Chem., Int. Ed.*, 2023, **62**, e202314420.
- Z. Gan, L. Wang, J. Cai, C. Guo, C. Chen, D. Li, Y. Fu, B. Zhou, Y. Sun, C. Liu, J. Zhou, D. Liu, W. Li and T. Wang, *Nat. Commun.*, 2023, **14**, 6297.
- L. Wang, C. Chen, Y. Fu, C. Guo, D. Li, J. Cheng, W. Sun, Z. Gan, Y. Sun, B. Zhou, C. Liu, D. Liu, W. Li and T. Wang, *Nat. Energy*, 2024, **9**, 208–218.
- Z. Yao, X. Cao, X. Bi, T. He, Y. Li, X. Jia, H. Liang, Y. Guo, G. Long, B. Kan, C. Li, X. Wan and Y. Chen, *Angew. Chem., Int. Ed.*, 2023, **62**, e202312630.
- J. Zhou, D. Li, L. Wang, X. Zhang, N. Deng, C. Guo, C. Chen, Z. Gan, C. Liu, W. Sun, D. Liu, W. Li, Z. Li, K. Wang and T. Wang, *Interdisciplinary Mater.*, 2023, **2**, 866–875.
- C. Liu, Y. Fu, J. Zhou, L. Wang, C. Guo, J. Cheng, W. Sun, C. Chen, J. Zhou, D. Liu, W. Li and T. Wang, *Adv. Mater.*, 2024, **36**, 202308608.
- H. Hu, S. Liu, J. Xu, R. Ma, Z. Peng, T. A. Dela Peña, Y. Cui, W. Liang, X. Zhou, S. Luo, H. Yu, M. Li, J. Wu, S. Chen, G. Li and Y. Chen, *Angew. Chem., Int. Ed.*, 2024, e202400086.
- H. Feng, N. Qiu, X. Wang, Y. Wang, B. Kan, X. Wan, M. Zhang, A. Xia, C. Li, F. Liu, H. Zhang and Y. Chen, *Chem. Mater.*, 2017, **29**, 7908–7917.
- D. Liu, B. Kan, X. Ke, N. Zheng, Z. Xie, D. Lu and Y. Liu, *Adv. Energy Mater.*, 2018, **8**, 1801618.
- V. Coropceanu, J. Cornil, D. A. da Silva Filho, Y. Olivier, R. Silbey and J.-L. Brédas, *Chem. Rev.*, 2007, **107**, 926–952.
- Z. Shuai, H. Geng, W. Xu, Y. Liao and J.-M. André, *Chem. Soc. Rev.*, 2014, **43**, 2662.
- R. S. Gurney, D. G. Lidzey and T. Wang, *Rep. Prog. Phys. Phys. Soc.*, 2019, **82**, 036601.
- W. Chen, M. P. Nikiforov and S. B. Darling, *Energy Environ. Sci.*, 2012, **5**, 8045.
- H.-C. Liao, C.-C. Ho, C.-Y. Chang, M.-H. Jao, S. B. Darling and W.-F. Su, *Mater. Today*, 2013, **16**, 326–336.
- D. P. McMahon, D. L. Cheung, L. Goris, J. Dacuna, A. Salleo and A. Troisi, *J. Phys. Chem. C*, 2011, **115**, 19386–19393.
- C. Zhang, J. Yuan, J. K. W. Ho, J. Song, H. Zhong, Y. Xiao, W. Liu, X. Lu, Y. Zou and S. K. So, *Adv. Funct. Mater.*, 2021, **31**, 2101627.
- W. Li, M. Chen, J. Cai, E. L. K. Spooner, H. Zhang, R. S. Gurney, D. Liu, Z. Xiao, D. G. Lidzey, L. Ding and T. Wang, *Joule*, 2019, **3**, 819–833.
- C. Yang, M. Jiang, S. Wang, B. Zhang, P. Mao, H. Y. Woo, F. Zhang, J. Wang and Q. An, *Adv. Mater.*, 2024, **36**, 2305356.
- A. M. Hiszpanski, R. M. Baur, B. Kim, N. J. Tremblay, C. Nuckolls, A. R. Woll and Y.-L. Loo, *J. Am. Chem. Soc.*, 2014, **136**, 15749–15756.
- J. Min, X. Jiao, I. Ata, A. Osvet, T. Ameri, P. Bäuerle, H. Ade and C. J. Brabec, *Adv. Energy Mater.*, 2016, **6**, 1502579.
- Y. He, N. Li, T. Heumüller, J. Wortmann, B. Hanisch, A. Aubele, S. Lucas, G. Feng, X. Jiang, W. Li, P. Bäuerle and C. J. Brabec, *Joule*, 2022, **6**, 1160–1171.
- J. J. van Franeker, S. Kouijzer, X. Lou, M. Turbiez, M. M. Wienk and R. A. J. Janssen, *Adv. Energy Mater.*, 2015, **5**, 1500464.
- Y. Liu, F. Liu, H.-W. Wang, D. Nordlund, Z. Sun, S. Ferdous and T. P. Russell, *ACS Appl. Mater. Interfaces*, 2015, **7**, 653–661.
- M. T. Fontana, H. Kang, P. Y. Yee, Z. Fan, S. A. Hawks, L. T. Schelhas, S. Subramaniyan, Y.-J. Hwang, S. A. Jenekhe, S. H. Tolbert and B. J. Schwartz, *J. Phys. Chem. C*, 2018, **122**, 16574–16588.
- C. Guo, Y. Fu, D. Li, L. Wang, B. Zhou, C. Chen, J. Zhou, Y. Sun, Z. Gan, D. Liu, W. Li and T. Wang, *Adv. Mater.*, 2023, **35**, e2304921.
- M. Li, C. An, T. Marszalek, M. Baumgarten, H. Yan, K. Müllen and W. Pisula, *Adv. Mater.*, 2016, **28**, 9430–9438.
- B. Lin, X. Zhou, H. Zhao, J. Yuan, K. Zhou, K. Chen, H. Wu, R. Guo, M. A. Scheel, A. Chumakov, S. V. Roth, Y. Mao, L. Wang, Z. Tang, P. Müller-Buschbaum and W. Ma, *Energy Environ. Sci.*, 2020, **13**, 2467–2479.
- B. Xie, K. Zhang, Z. Hu, H. Fang, B. Lin, Q. Yin, B. He, S. Dong, L. Ying, W. Ma, F. Huang, H. Yan and Y. Cao, *Solar RRL*, 2020, **4**, 1900385.
- Z. Yao, Z. Wang, H. Wu, Y. Lu, Q. Li, L. Zou, J. Wang and J. Pei, *Angew. Chem., Int. Ed.*, 2020, **132**, 17620–17624.
- M. Zhang, X. Guo, W. Ma, H. Ade and J. Hou, *Adv. Mater.*, 2015, **27**, 4655–4660.
- K. Jin, Z. Xiao and L. Ding, *J. Semicon.*, 2021, **42**, 060502.
- R. Österbacka, C. P. An, X. M. Jiang and Z. V. Vardeny, *Science*, 2000, **287**, 839–842.
- M. D. Heinemann, K. von Maydell, F. Zutz, J. Kolny-Olesiak, H. Borchert, I. Riedel and J. Parisi, *Adv. Funct. Mater.*, 2009, **19**, 3788–3795.
- N. M. B. Neto, M. D. R. Silva, P. T. Araujo and R. N. Sampaio, *Adv. Mater.*, 2018, **30**, 1705052.
- D. T. Scholes, P. Y. Yee, J. R. Lindemuth, H. Kang, J. Onorato, R. Ghosh, C. K. Luscombe, F. C. Spano, S. H. Tolbert and B. J. Schwartz, *Adv. Funct. Mater.*, 2017, **27**, 1702654.
- J. Yamamoto and Y. Furukawa, *J. Phys. Chem. B*, 2015, **119**, 4788–4794.
- D. Rosu, L. Rosu and C. N. Cascaval, *Polym. Degrad. Stab.*, 2009, **94**, 591–596.
- Y. Wang, J. Luke, A. Privitera, N. Rolland, C. Labanti, G. Londi, V. Lemaur, D. T. W. Toolan, A. J. Sneyd, S. Jeong,

- D. Qian, Y. Olivier, L. Sorace, J.-S. Kim, D. Beljonne, Z. Li and A. J. Gillett, *Joule*, 2023, 7, 810–829.
- 42 R. Chang, J. H. Hsu, W. S. Fann, J. Yu, S. H. Lin, Y. Z. Lee and S. A. Chen, *Chem. Phys. Lett.*, 2000, 317, 153–158.
- 43 F. C. Spano and C. Silva, *Annu. Rev. Phys. Chem.*, 2014, 65, 477–500.
- 44 T. Wang, A. J. Pearson, A. D. F. Dunbar, P. A. Staniec, D. C. Watters, H. Yi, A. J. Ryan, R. A. L. Jones, A. Iraqi and D. G. Lidzey, *Adv. Funct. Mater.*, 2012, 22, 1399–1408.